Incorporation of Distance-Protection Tripping to the Direct Methods for Transient Stability Assessment

Valentin Azbe, Rafael Mihalic
Faculty of electrical engineering
University of Ljubljana
Ljubljana, Slovenia
valentin.azbe@fe.uni-lj.si

***Abstract*—Protection security assessments are an emerging part of dynamic security assessments. This should be considered also when direct methods are applied for transient stability assessment of electric-power systems, i.e., protection devices should be properly considered. This is currently not always possible because present direct methods do not involve intentional delayed tripping of distance protection. This paper presents how to overcome this inconsistency. The time component was extracted from the Lyapunov energy function applied in the direct method. The speed of the transformation between the kinetic and the potential parts of the energy function was the key parameter in assessing the time interval on the post-fault trajectory inside various distance protection zones. From these time intervals an unwanted trip of distance protection relay during the power swing can be identified. The correctness of the newly proposed method was verified by a comparison of the direct method and the well-known time-domain numerical simulation method for a single-machine infinite-bus test system.**

Index Terms ***—transient stability; distance protection; direct methods; energy functions.***

I. Introduction

In past research [1]-[3] it has been established that in the process of transient stability assessments for electric-power systems (EPSs) the protection devices can have an important role due to the possibility of line trippings. Firstly protection devices were only considered in steady-state analyses [1]. However, this has changed in recent years, as now they are also considered in time-domain numerical simulations for transient stability assessments [2], [3].

Dynamic analyses of large interconnected power systems require a lot of computational power. Despite the rapid increase of the computer-processor power the time-domain numerical simulation of power-system dynamics is still quite a time-consuming task. An alternative to the time-domain simulations is the direct methods that apply Lyapunov energy functions. Their advantage is, besides the speed, a quantitative assessment of the stability margins.

Consideration of protection devices in direct methods for transient-stability assessment was partly performed for overcurrent and differential protection [4]. Distance protection is partly analyzed in [4] as well, but only the detection of impedance inside the tripping zones is considered, without any time components that define the activation of the time-delayed zones. This paper provides an answer to the question of how to assess the intentional delayed tripping of distance protection when direct methods are applied.

II. Direct Method for a Transient Stability Assessment Based on a Lyapunov Energy Function

In the presented work the behavior of distance protection is incorporated into the direct method for the transient stability assessment. The latter is based on the Lyapunov energy function. It is a well-known method, developed in the 1980s, described in [5], [6], and applied for various dynamic analyses of EPSs, e.g. [7], [8]. For the readers' convenience the basics of the direct method and the Lyapunov energy functions—relevant to our derivations—are briefly described in this section.

In [5], the Lyapunov energy function V_t is constructed on the structure-preserving frame and is defined as the sum of the so-called "kinetic energy" and "potential energy":

$$V_\mathrm{t} = V_\mathrm{k} + V_\mathrm{p} + \mathrm{K} \tag{1}$$

For an EPS with n generators, the V_k in (1) is the kinetic energy defined as:

$$V_\mathrm{k} = \sum_{i=1}^{n} \frac{1}{2} \cdot \mathrm{m}_i \cdot \omega_i^2 \tag{2}$$

where m_i is the generator inertia coefficient of the i-th generator and ω_i is the difference between the rotor velocity of the i-th generator and the synchronous velocity. It should be stressed that according to this definition, in the steady state all ω_i (and consequently V_k) are equal to 0. Only during transients—when the rotors accelerate and/or decelerate—does V_k differ from 0. The potential energy V_p in (1) is an extensive function that depends on the rotor angles of all the generators and on other parameters of the EPS, like the impedances, the voltages and the generators' mechanical

powers. The definition of V_p is not included in this paper; however, it is calculated according to [5] and [6]. In a simplified way V_p can be treated as the capability of the EPS to receive electric power from the generators. The value of K in (1) is an arbitrary constant, usually chosen so that it places the origin of (1) at zero.

The principle of transient stability assessment (i.e. the assessment of critical clearing time) with the application of direct methods is to compare the V_t from (1) along the fault-on trajectory (i.e., the trajectory of rotor angles under a sustained fault) with the potential energy V_p from (1) at the border of the stable area. The critical clearing time (CCT) is determined as the point at which V_t becomes equal to the potential energy V_p at the border of the stable area (it means that all the kinetic energy will be transformed to the potential one). Various points at the border of the stable area can be considered for this comparison. In this study the potential-energy boundary surface (PEBS) method [6] is used.

In this paragraph the meaning of the "potential energy of the post-fault system along the fault-on trajectory" is described. The fault-on trajectory (i.e., the trajectory with a sustained fault) is calculated firstly using a time-domain numerical simulation. With this numerical simulation the generator's rotor speed ω and angle δ are obtained (3rd and 4th column in Table I). It should be stressed that the rotor speed ω is the difference between the rotor velocity and the synchronous velocity. Then the rotor angles δ from the fault-on trajectory (i.e., 4th column in Table I) are taken as the initial conditions for the calculation of the post-fault power-flows at each point of the fault-on trajectory (i.e., for each row in Table I). With this calculation the voltage magnitudes V and the angles Θ of each node are obtained (5th, 6th, 7th, 8th … column in Table I). The voltages from these power-flow calculations are considered for the calculation of the potential energy V_p (before-the-last column in Table I). In this way the potential energy of the post-fault system along the fault-on trajectory is determined. In Table I also the kinetic energy V_k (2) and t_{return} (16) (i.e., the final result of this paper) are included.

TABLE I

THE DATA OF THE POST-FAULT SYSTEM ALONG THE FAULT-ON TRAJECTORY

	Fault-on trajectory			Post-fault system						
n	t [s]	ω [rad/s]	δ [rad]	V_1 [pu]	Θ_1 [rad]	V_2 [pu]	Θ_2 [rad]	V_k	V_p	t_{return} [s]
1	0	0	0,165543	1,06107	0,073696	1,00809	0,0071172	0	0	0
2	0,001	0,022362	0,165554	1,06106	0,073701	1,00809	0,0071177	4,37E-06	7,96E-08	0,0973594
3	0,002	0,044723	0,165587	1,06106	0,073716	1,00809	0,0071191	1,75E-05	3,20E-07	0,1546704

III. DIRECT METHOD FOR ASSESSING THE UNWANTED TRIPPING OF THE DISTANCE PROTECTION

The newly proposed method for the detection of unwanted distance-protection tripping during power swings is based on the course of the potential and kinetic energies along the fault-on trajectory. The first step is the determination of the time points on the fault-on trajectory, in which the impedances (i.e., the impedances as measured by the protection devices on the post-fault system immediately after the fault clearing) enter particular protection zones for each of the protection devices. The second step is a determination of the durations of the post-fault trajectory persisting inside particular protection zones for each of the protection devices. The durations in question are calculated from the speed of the transformation between the kinetic and potential parts of the energy function. The method is presented step-by-step in the following subsections.

A. Determination of the highest potential energy

After a fault clearance, the sum of the kinetic and potential energies V_t (1) is constant (because a lossless system is considered) [5]. This means that the kinetic energy gained during a fault is transformed into potential energy. Consequently, the highest potential energy V_{high} after the fault clearing is reached when all the kinetic energy is transformed into potential energy. So, V_{high} can be calculated as the sum of the kinetic and potential energies V_k+V_p at the moment of fault clearing.

B. Determination of the rotor deceleration

The time needed to reach V_{high} after the fault clearing depends on the speed of the transformation of the kinetic energy to the potential energy. Having in mind that the velocity ω, considered in the kinetic part of the energy function (2), is the time derivative of rotor angle δ, the deceleration of the rotor can be clearly presented using a V_p/δ diagram. Since the dependence of V_p on δ in (1) is not defined explicitly, but only implicitly, the V_p/δ diagram can only be obtained numerically. In further subsections the transformation of the kinetic energy to potential energy is described for a single-machine infinite-bus (SMIB) system. An example of a V_p/δ diagram for a SMIB system is presented in Fig. 1.

The slope of the potential energy over a short interval from δ_1 to δ_2 may be considered constant and can be defined as:

$$k = \frac{V_{p2} - V_{p1}}{\delta_2 - \delta_1} \tag{3}$$

In this case the linear dependence of V_p on δ can be considered for this interval:

$$V_p(\delta) = V_{p1} + k \cdot \delta \tag{4}$$

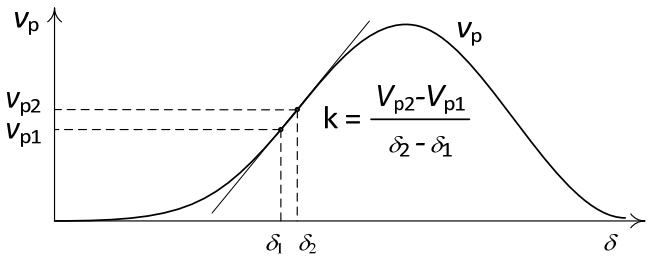

Fig. 1. Slope of the potential energy in a V_p/δ diagram.

According to the theory of the Lyapunov energy function the sum of the kinetic and potential energies (in a lossless system) is a constant. Consequently, the sum of the time

derivative of the kinetic energy and the time derivative of the potential energy also equals 0:

$$\frac{\mathrm{d}V_{\mathrm{k}}(\omega)}{\mathrm{d}t}+\frac{\mathrm{d}V_{\mathrm{p}}(\delta)}{\mathrm{d}t}=0 \tag{5}$$

Considering (2) and (4), (5) can be rewritten as:

$$\frac{\mathrm{d}\left(\frac{1}{2}\cdot \mathrm{m}\cdot\omega^{2}\right)}{\mathrm{d}t}+\frac{\mathrm{d}\left(\mathrm{V}_{\mathrm{p1}}+\mathrm{k}\cdot\delta\right)}{\mathrm{d}t}=0 \tag{6}$$

Since m and V_{p1} are constant and ω is equal to the time derivative of δ, (6) can be further simplified as:

$$\begin{aligned}&\frac{1}{2}\cdot \mathrm{m}\cdot\frac{\mathrm{d}\left(\omega^{2}\right)}{\mathrm{d}t}+\mathrm{k}\cdot\frac{\mathrm{d}\delta}{\mathrm{d}t}=\\&2\cdot\frac{1}{2}\cdot \mathrm{m}\cdot\omega\cdot\frac{\mathrm{d}\omega}{\mathrm{d}t}+\mathrm{k}\cdot\omega=\\&\mathrm{m}\cdot\frac{\mathrm{d}\omega}{\mathrm{d}t}+\mathrm{k}=0\end{aligned} \tag{7}$$

From (7), the deceleration can be denoted as:

$$-\frac{\mathrm{d}\omega}{\mathrm{d}t}=\mathrm{k}/\mathrm{m} \tag{8}$$

C. Rotor velocity over a short interval with constant deceleration

In addition to the deceleration (8) the velocity at the beginning and at the end of the short interval from δ_1 to δ_2 according to Fig. 1 can also be obtained. Since the sum of the kinetic and potential energies is a constant and considering (2) we can write:

$$\frac{1}{2}\cdot \mathrm{m}\cdot\omega_{0}^{2}-\frac{1}{2}\cdot \mathrm{m}\cdot\omega_{1}^{2}=V_{\mathrm{p1}}-V_{\mathrm{p0}} \tag{9}$$

where ω_1 and V_{p1} stand for the rotor velocity and the potential energy, respectively, at the beginning of the interval, while ω_0 and V_{p0} stand for the rotor velocity and the potential energy, respectively, at the point of the fault clearing. Similarly, for the end of the interval we can write:

$$\frac{1}{2}\cdot \mathrm{m}\cdot\omega_{0}^{2}-\frac{1}{2}\cdot \mathrm{m}\cdot\omega_{2}^{2}=V_{\mathrm{p2}}-V_{\mathrm{p0}} \tag{10}$$

where ω_2 and Vp2 stand for the rotor velocity and the potential energy, respectively, at the end of the interval. From (9) the velocity at the beginning of the interval can be determined as:

$$\omega_{1}=\sqrt{\omega_{0}^{2}-\frac{2}{\mathrm{m}}\left(V_{\mathrm{p1}}-V_{\mathrm{p0}}\right)} \tag{11}$$

Similarly, from (10) the velocity at the end of the interval can be determined as:

$$\omega_{2}=\sqrt{\omega_{0}^{2}-\frac{2}{\mathrm{m}}\left(V_{\mathrm{p2}}-V_{\mathrm{p0}}\right)} \tag{12}$$

D. Duration of a short interval with constant deceleration

When the deceleration is a constant and the velocity at both ends of a short interval is known, the duration of this interval can be easily obtained since the deceleration is defined as the change of velocity over the time. Considering (8), (11) and (12), the duration of the short interval can be determined as:

$$\begin{aligned}t&=\frac{\omega_{1}-\omega_{2}}{\mathrm{k}/m}=\\&=\frac{\sqrt{\omega_{0}^{2}-\frac{2}{\mathrm{m}}\left(V_{\mathrm{p1}}-V_{\mathrm{p0}}\right)}-\sqrt{\omega_{0}^{2}-\frac{2}{\mathrm{m}}\left(V_{\mathrm{p2}}-V_{\mathrm{p0}}\right)}}{\mathrm{k}/m}\end{aligned} \tag{13}$$

The duration of the last interval, where the potential energy reaches its maximum (and the kinetic energy decreases to 0) somewhere within this interval, must be considered separately because the post-fault trajectory does not reach the end of the interval. Only the part of this last interval from its beginning to the "V_{high}" point, at which the highest potential energy V_{high} is achieved, should be considered. In this "V_{high}" point the kinetic energy equals 0, which means that the rotor velocity ω is also 0. Consequently, at the "V_{high}" point the second square root in (13) equals 0 and the duration of this last interval (denoted as the n-th interval) can be calculated as:

$$t_{\mathrm{n}}=\frac{\sqrt{\omega_{0}^{2}-\frac{2}{\mathrm{m}}\left(V_{\mathrm{p(n-1)}}-V_{\mathrm{p0}}\right)}}{\mathrm{k_n}/m} \tag{14}$$

where $V_{\mathrm{p(n-1)}}$ stands for the potential energy at the beginning of n-th interval and $\mathrm{k_n}$ stands for the slope of the potential energy in the n-th interval from its beginning to the point of the highest potential energy V_{high}. It should be noted that although the intervals can be very short, the contribution of this last n-th interval to the total duration is significant due to the low rotor velocity.

E. Summation of short intervals

In order to obtain the duration from the fault clearance to the point of the highest potential energy V_{high}, the durations of all the short intervals (13) between these two points should be summarized and the last interval (14) should be added:

$$\begin{aligned}t_{\text{post-fault}}=&\sum_{i=1}^{\mathrm{n-1}}\frac{\sqrt{\omega_{0}^{2}-\frac{2}{\mathrm{m}}\left(V_{\mathrm{p}(i\text{-}1)}-V_{\mathrm{p0}}\right)}-\sqrt{\omega_{0}^{2}-\frac{2}{\mathrm{m}}\left(V_{\mathrm{p}(i)}-V_{\mathrm{p0}}\right)}}{\mathrm{k}_{i}/m}\\&+\frac{\sqrt{\omega_{0}^{2}-\frac{2}{\mathrm{m}}\left(V_{\mathrm{p(n-1)}}-V_{\mathrm{p0}}\right)}}{\mathrm{k_n}/m}\end{aligned} \tag{15}$$

where n stands for the number of intervals from the fault clearance to the point of the highest potential energy, $V_{\mathrm{p}(i\text{-}1)}$ stands for the potential energy at the beginning of the i-th interval, $V_{\mathrm{p}(i)}$ stands for the potential energy at the end of the i-th interval and k_i stands for the slope of the potential energy in

the i-th interval. The last n-th interval is included in (15) as a separate element outside the summation because of the different consideration described in the previous subsection.

F. *Time interval of the post-fault trajectory persisting inside the protection zone*

Using (15) the time interval $t_{\text{post-fault}}$ from the fault clearing to the moment when the post-fault trajectory reaches the highest potential energy V_{high} is calculated. After the highest potential energy V_{high} (at which V_{k} equals 0) is reached, the rotor angle and the potential energy begin to decrease, the rotor speed becomes negative and the kinetic energy increases. The post-fault trajectory on this "return" path in the SMIB system follows the same system operating points (in the opposite direction) as on the way from the fault clearing to the highest potential energy V_{high}, because the trajectory of the SMIB system is uniformly given, while in multi-machine systems this "return" path differs to a greater or lesser extent. As the same physical laws are valid for this "return" trajectory, the time for this "return" trajectory to reach a potential energy that equals the potential energy at fault clearing is equal to $t_{\text{post-fault}}$. So the duration of the operating point leaving the fault-clearing point and coming back again to the same operating point can be evaluated as twice the value of $t_{\text{post-fault}}$. This is valid for the SMIB system, while for multi-machine systems some deviations are expected due to the various possible paths of the post-fault trajectory.

Considering these facts, for each point on the fault-on trajectory (i.e., for any fault-clearing time) the time of the post-fault system's operating point to return to the same operating point (i.e., the point of the fault clearing) can be assessed as:

$$t_{\text{return}} = 2 \cdot t_{\text{post-fault}} \tag{16}$$

With this calculation the last column in Table I is obtained.

Eq. (16) is represented in Fig. 2.

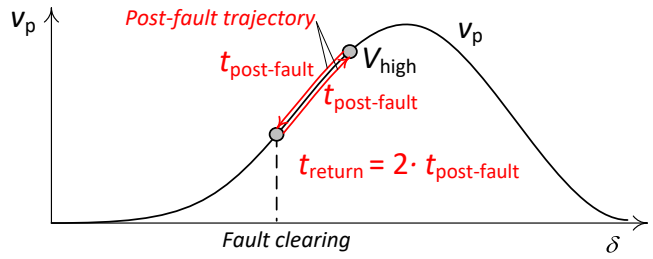

Fig. 2. Definition of the return time t_{return} in (16).

With the above calculation the last column in Table I is obtained. Of all the times t_{return} on the fault-on trajectory (i.e., the last column in Table I) the most informative are those that are obtained for the clearing times when the impedance immediately after the fault clearing "jumps" on the border of a particular protection zone. These times t_{return} represent the exact time intervals of the post-fault trajectory persisting inside a particular protection zone—for the case when the impedance immediately after the fault clearing is at the border of a particular protection zone—and are used as the indices for an assessment of unwanted tripping.

G. *Presentation of the indices for the assessment of unwanted tripping*

To calculate (16) only a single calculation for each point on the fault-on trajectory can be applied for all distance protection devices and the results of this calculation can be presented like the diagram in Fig. 3. In this diagram the return time t_{return} from (16) is presented with respect to the fault clearing time t_{FC}. Two distance protection devices are considered within the diagram and marked with #1and #2, respectively, and for each of these devices the entrance to the specific zone is marked with the index: PSC for the power-swing characteristic, Z3 for zone 3, Z2 for zone 2 and Z1 for zone 1. The time on the fault-on trajectory when the post-fault impedance, measured by the distance protection device, enters the protection zone is, for each of the two protection devices, denoted as t_{enter}. For each protection device and each zone it is assumed that the fault is cleared on its own t_{enter} and the duration of the return time according to (16) is in Fig. 3 denoted as t_{return}. For zones 1 only t_{enter} is calculated, while t_{return} is not important due to the immediate trip in zone 1. The critical clearing time (CCT) is also presented in the diagram in order to present the border of the transient stability. It is assumed that the tripping of the protection devices beyond this border is not relevant because the system will become unstable anyway. However, the proximity of t_{enter} to a CCT gives valuable information about the dynamic security margin, even if it is beyond a CCT.

The times t_{enter} and t_{return} for each protection device and each zone are the final results of the newly proposed method and can be applied as the indices for an assessment of the unwanted tripping during power swings. The assessment of the unwanted tripping according to these indices and according to the delay times of the distance protection devices is described using the numerical example in the next section.

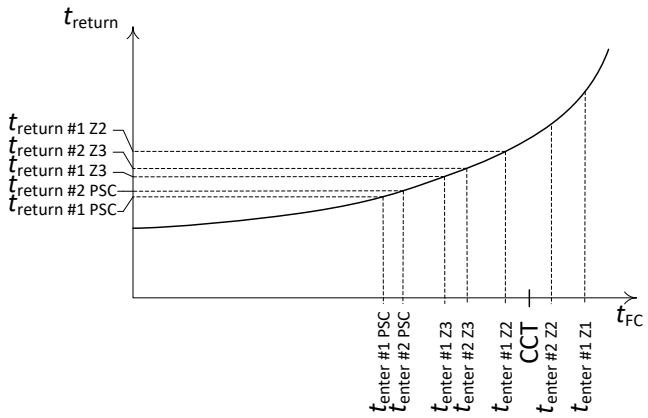

Fig. 3. Principle of the presentation of parameters for an unwanted tripping assessment.

H. Consideration of a multi-machine EPS

In a multi-machine EPS the energy, speed and deceleration are calculated along the fault-on trajectory. The potential energy in the SMIB system presented in Fig. 1 becomes a multi-dimensional surface. For our derivations it can be transformed into a two-dimensional diagram of the potential energy along the fault-on trajectory, where the rotor angle δ in the V_p/δ diagram and in equations (3) to (7) is replaced by a vector sum of all n rotor angles in the n-dimensional coordinate system and is calculated as:

$$\delta_m = \sqrt{\delta_1^2 + \delta_2^2 + ... + \delta_n^2} \tag{17}$$

where n is the number of all the generators in the system and m is the index that denotes the multi-machine system. Similarly, the speed of the rotor in (6) to (15) should be calculated as the vector sum of all n rotor speeds in the n-dimensional coordinate system:

$$\omega_m = \sqrt{\omega_1^2 + \omega_2^2 + ... + \omega_n^2} \tag{18}$$

where the index m is again used to denote the multi-machine system. In order to obtain a deceleration (8) after the fault clearance for a multi-machine system (in the direction of a fault-on trajectory), the kinetic energy must be defined with the use of the rotor speed (18). However, this kinetic energy must be equal to the sum of all the kinetic energies of all n generators:

$$\frac{1}{2} m_m \cdot \omega_m^2 = \frac{1}{2} m_1 \cdot \omega_1^2 + \frac{1}{2} m_2 \cdot \omega_2^2 + ... + \frac{1}{2} m_n \cdot \omega_n^2 \tag{19}$$

Consequently, the generator inertia coefficient m_m in (19)—which is some kind of common inertia coefficient for all the generators in the system—depends not only on the inertia coefficients of all the generators, but also on the speed of the generators, and can be calculated from (18) and (19) as:

$$m_m = \frac{m_1 \cdot \omega_1^2 + m_2 \cdot \omega_2^2 + ... + m_n \cdot \omega_n^2}{\omega_1^2 + \omega_2^2 + ... + \omega_n^2} \tag{20}$$

The common inertia coefficient m_m is obviously not a constant. But over a short time interval—for which the deceleration (8) is calculated from the time derivative in (7)—it can be (and must be) considered as a constant. In the equations (9) to (15) m_m is also considered as a sectional-constant, i.e., a constant inside each short time interval.

To conclude, the equations (3) to (16) that are valid for a SMIB system can also be applied for a multi-machine system; however, the rotor angle δ, the rotor speed ω and the inertia coefficient m in (3) to (16) must be replaced by the rotor angle δ_m (17), the rotor speed ω_m (18) and the inertia coefficient m_m (20).

IV. Numerical example

A. SMIB test system

The newly proposed method was firstly tested on a longitudinal SMIB system. Because the fault-on and post-fault trajectories of the SMIB system are uniformly given, the CCT, times t_{enter} and t_{return} should be the same as the one obtained using the time-domain simulations. However, exactly the same system model in both the simulation and the direct method has to be applied.

The test system is presented in Fig. 4. This longitudinal system consists of a generator connected to an infinite bus via a 500-kV power line. The generator is presented as a classic model. Its initial voltage at BUS1 was set to a 1.1 p.u. at 4°. The disturbance is a three-phase fault near BUS2, see Fig. 4, and is assumed to be eventually cleared, i.e., the system's post-fault configuration is identical to the pre-fault one. The distance protection DP1 in Fig. 4 detects this fault in zone 2 and the behavior after the fault clearing is analyzed for this device.

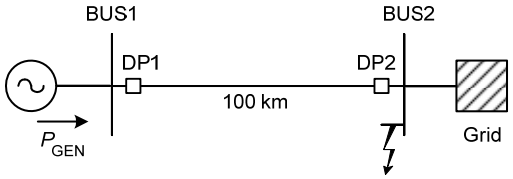

Fig. 4. Longitudinal test-system scheme

Because the Lyapunov energy function is, in general, valid only for a lossless system, ohmic resistances are omitted in the numerical simulations.

The CCT, times t_{enter} and t_{return} for the fault near BUS2 were obtained, firstly, with the repetition of time-domain numerical simulation and, secondly, using a newly proposed method. The results obtained with both methods are presented in Table II. The results are identical and this confirms the correctness of the proposed method. From the results it can be seen that without any consideration of distance protection the CCT to maintain the transient stability would be 419 ms. With a consideration of distance protection it is clear that if the fault is longer than 407 ms the impedance will be inside zone 3 for 246 ms. Because during the fault the impedance is inside zone 2, the timer of the distance protection has started immediately after the fault and the total time of the timer before the exit from zone 3 will be equal to the sum of t_{enter} and t_{return} for zone 3, i.e., 653 ms. If the time delay for zone 3 is set to 600 ms, the distance protection will trip the line. If the clearing time is less than 407 ms, the impedance immediately after the fault clearing will be outside zone 3 and the timer will reset, but during the power swing it will be started again when the post-fault trajectory will enter zone 3. However, according to t_{return} for zone 3, the duration inside zone 3 (and the time on the timer) will be shorter than 246 ms and consequently no trip will occur.

The times t_{enter} for zone 2 and zone 1 are longer than the CCT; consequently, the t_{return} for these two zones cannot be calculated because of the no-return trajectory.

TABLE II.

CCTs, TIMES T_{ENTER} AND T_{RETURN} OBTAINED IN A LONGITUDINAL SYSTEM.

	Direct method		Numerical simulation	
	t_{enter}	t_{return}	t_{enter}	t_{return}
CCT [ms]	419	560	419	560
PSC [ms]	376	161	376	161
Z3 [ms]	407	246	407	246
Z2 [ms]	428	-	428	-
Z1 [ms]	449	-	449	-

B. *IEEE 3-machine 9-bus test system*

The second test system is the IEEE 3-machine 9-bus test system, for which the data can be found in [9]. The system has 6 lines and each line is equipped with distance protection relays at both ends. The system is presented in Fig. 5. The disturbance is a three-phase fault near bus 7 and is assumed to be cleared by DPXX, i.e., the system's post-fault configuration is identical to the pre-fault one. The active power of the generators in the steady state before the fault are intentionally set quite low in order to obtain a case where the time t_{enter} for the power-swing characteristic is shorter than the CCT. In the area of the nominal active power of the generators the t_{enter} for the power-swing characteristic would be longer than the CCT.

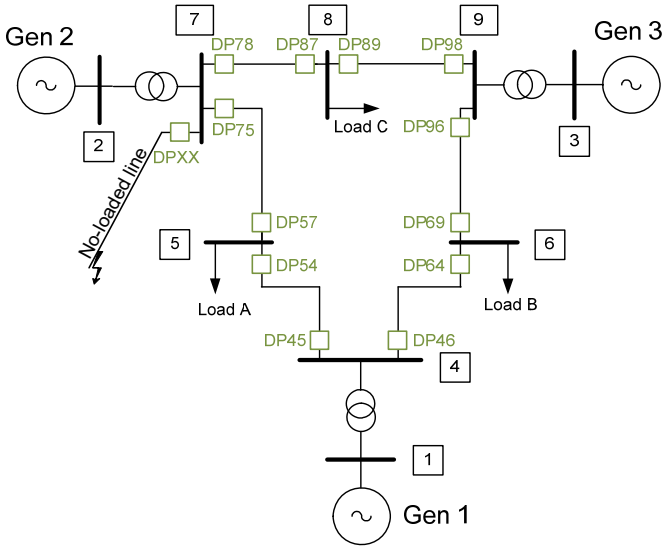

Fig. 5. An IEEE nine-bus test system.

For each of the distance protection relays its impedance was calculated on the basis of post-fault voltages and currents along the fault-on trajectory (the trajectory of the rotor angles during a sustained fault). However, the distance protection DP75 is the only distance protection relay where the calculated impedance after the fault clearing was inside the power-swing characteristic for fault-clearing times less than the CCT.

The CCT, times t_{enter} and t_{return} for the fault near bus 7 were obtained, firstly, using the newly proposed method and, secondly, with the repetition of the time-domain numerical simulation. The results obtained with both methods for the distance protection DP75 are presented in Table III. Because in multi-machine systems the fault-on trajectory and the post-fault trajectory do not follow the same path exactly, some differences are expected in times t_{return}. However, these differences are quite small for the example in question: t_{return} for zone 3 obtained with the proposed direct method is 202 ms, while with the time-domain numerical simulation t_{return} is 9 ms longer, i.e., 211 ms. The results obtained by time-domain numerical simulations are more accurate than those obtained by a direct method; however, direct methods are faster. In the subsequent description the results from the direct method will be applied as these results are obtained using the proposed method in this paper.

From the results in Table III it can be seen that without any consideration of distance protection the CCT to maintain the transient stability would be 758 ms. With a consideration of distance protection it is clear that if the fault clearing time is longer than 737 ms the impedance of DP75 will be inside zone 3 longer than 202 ms. We assume DP75 is a distance protection relay with a general timer that picks-up undirectional with zone 3. This is why in this example the timer has started with the measured impedance at fault inception inside zone 1 (reverse direction – DP75 do not trip). After 737 ms (tenter) the measured impedance remains inside zone 3 for 202 ms (treturn). The timer results in the sum of tenter and treturn being 939 ms. If the time delay for zone 3 is set below that value (e.g., to 850 ms), the distance protection will trip the line unwanted. This example shows that in spite of the fact that the CCT is 758 ms, the stability of the system might be lost due to unwanted line tripping if the fault clearing time is longer than 737 ms.

If the clearing time is less than 737 ms, the impedance immediately after the fault clearing will be outside zone 3 and the general timer will reset. During the power swing the general timer will be started again when the post-fault trajectory will enter zone 3. However, the duration inside zone 3 (which corresponds to the general timer) will be shorter than 202 ms and consequently no unwanted trip will occur.

If the clearing time is longer than 737 ms, the impedance immediately after the fault clearing will be inside zone 3 and the general timer will not reset. The time interval for the post-fault trajectory persisting inside the zone will be longer than the treturn (202 ms) and unwanted tripping will occur. The times tenter for zone 2 and zone 1 are longer than the CCT; consequently, the treturn for these two zones is infinite because of the no-return post-fault trajectory.

TABLE III.

CCTs, TIMES T_{ENTER} AND T_{RETURN} FOR DP75 OBTAINED IN A MULTI-MACHINE TEST SYSTEM.

	Direct method		Numerical simulation	
	t_{enter}	t_{return}	t_{enter}	t_{return}
CCT [ms]	758	∞	760	∞
PSC [ms]	707	140	707	152
Z3 [ms]	737	202	737	211
Z2 [ms]	785	∞	785	∞
Z1 [ms]	809	∞	809	∞

The main purpose of these calculations was to demonstrate the proposed method on a multi-machine system. According to the results the time delays of the tripping zones can be revised in order to avoid unwanted tripping during power swings and to improve the post-fault system stability and security.

V. Conclusions

The method proposed combines the direct method for transient stability assessment with an assessment of the unwanted tripping of distance-protection relays during power swings. The method applies the Lyapunov energy function and, consequently, it enables a rapid calculation. This opens the option for future speed-critical applications of dynamic protection security assessment. The proposed method is presented step-by-step and is validated using a comparison with the results from time-domain numerical simulations on a SMIB test system. The applicability of the proposed method is also presented for a multi-machine systems. The results enable the system operator to improve the protection relay performance in terms of a higher dynamic system security.

References

[1] J. Jaeger and R. Krebs, "Protection Security Assessment - An important Task for Blackout Prevention," in Proc. 2010 IEEE Power Engineering Society Powercon Conf., pp. 1-6.

[2] J. Jaeger, T. Keil, A. Dienstbier, P. Lund and R. Krebs, “Network security assessment - An important task in distribution systems with dispersed generation” in Proc. 20th International Conference and Exhibition on Electricity Distribution CIRED 2009, Part 1, pp 1-4.

[3] C. Romeis and J. Jaeger, "Dynamic Protection Security Assessment, a Technique for Blackout Prevention," in Proc. 2013 IEEE Power Engineering Society Powertech Conf., pp. 1-6.

[4] G. Ziegler, Numerical Distance Protection, Publicis Publishing, 2011.

[5] Th. Van Cutsem, M. Ribbens-Pavella, "Structure preserving direct methods for transient stability analysis of power systems," Proc. of 24th Conf. on Decision and Control, Dec. 1985, pp 70-77.

[6] M. A. Pai, Energy Function Analysis For Power System Stability, Kluwer Academic Publishers, 1989.

[7] V. Azbe, U. Gabrijel, R. Mihalic and D. Povh, "The Energy Function of a General Multimachine System with a Unified Power Flow Controller," IEEE Trans. Power Systems, vol. 20, no. 3, pp. 1478–1485, Aug. 2005.

[8] V. Azbe and R. Mihalic, "The Control Strategy for an IPFC Based on the Energy Function," IEEE Trans. Power Systems, vol. 23, no. 4, pp. 1662–1669, Nov. 2008.

[9] P. M. Anderson, A. A. Fouad, *Power System Control and Stability*, IEEE Press Power Systems Engineering Series, Revised Printing, 1999.